JOURNAL OF APPLIED ELECTROCHEMISTRY 23 (1993) 684–692

Studies of the hydrogen evolution reaction on lanthanum phosphate-bonded composite nickel–ruthenium electrodes in 1 M alkaline solutions

H. DUMONT, P. LOS*, A. LASIA, H. MÉNARD

Département de Chimie, Université de Sherbrooke, Sherbrooke, Québec, Canada J1K 2R1

L. BROSSARD

Institut de Recherche d'Hydro-Québec (IREQ), 1800 Montée Ste-Julie, Varennes, Québec, Canada J3X 1S1

Received 15 June 1992; revised 10 October 1992

The electrocatalytic properties of lanthanum phosphate-bonded composite nickel–ruthenium electrodes for the hydrogen and oxygen evolution reactions were studied in 1 M KOH at 25° C. Ruthenium was chemically deposited on nickel powder particles prior to polymerization of Ni/Ru powder with lanthanum phosphate. X-ray diffraction (XRD), X-ray fluorescence (XRF), BET, differential thermal analysis (DTA), scanning electron microscopy (SEM), EDX and u.v./vis. spectrophotometry were used to investigate the composition, morphology and characteristics of the electrodes. The influence of the ruthenium content and polymerization temperature on the electrocatalytic activity for hydrogen and oxygen evolution were studied. The mechanism and kinetics of the hydrogen evolution reaction (HER) were investigated using both steady-state polarization and a.c. impedance techniques.

1. Introduction

High surface area nickel-based electrodes are known to be active electrocatalysts in the electrolysis of hot concentrated alkaline water solutions. These electrodes may be obtained through sintering, vacuum, or plasma spray deposition, electrodeposition, electrocodeposition, or high-temperature deposition [1–9].

A new process of cementing metallic powders to produce high surface area electrodes has been recently reported [10–13]. Aluminium and lanthanum phosphate-bonded nickel (LPBN) electrodes were produced with spiky filamentary nickel powders. The electrodes containing 2 wt % $LaPO_4$ were stable in hot 30 wt % alkaline solution during 200 h of electrolysis. The deposition of a metallic element onto the nickel particles may be beneficial for the hydrogen evolution reaction (HER) if the deposited metal has low overvoltage for the HER and is chemically stable in contact with alkaline solutions. However, strong influence of the preparation conditions, particularly the polymerization temperature on the LPBN and LPBN–Rh electrode activity, was established in a previous paper [13]. It should be noted that the LPBN electrode obtained by the deposition of a small amount of rhodium on the nickel powder possesses high electrocatalytic activity for the HER in alkaline solutions.

The aim of this work is to produce very active LPBN electrodes for water electrolysis by chemically depositing ruthenium on the spiky filamentary nickel powder. Ruthenium is recognized as being a very active metal for the HER, and it is also chemically stable in alkaline solution [14, 15].

2. Theory

The HER occurs according to the following reactions [8, 9]:

$$H_2O + e^- + M = M\text{–}H_{ads} + OH^- \quad (1)$$

$$M\text{–}H_{ads} + H_2O + e^- = H_2 + OH^- + M \quad (2)$$

$$2\,M\text{–}H_{ads} = H_2 + 2M \quad (3)$$

The mechanism of the HER was studied to explain the influence of the structure and the composition of nickel–ruthenium electrodes on their electroactivity. Electrochemical studies were carried out using the a.c. impedance and Tafel curve methods. The LPBN electrodes are rough and there is considerable difference between the geometric and active surface areas. Therefore, the current density is not uniformly distributed, which causes a frequency dispersion of impedance results. The successful fitting of a.c. measurement data of rough electrodes could be realized using constant phase element (CPE) or fractal models [16–21]. The constant phase element is defined by the following equation [21]:

$$Z_{CPE} = \frac{1}{T(j\omega)^{\phi}} \quad (4)$$

where ω is the angular frequency, the ϕ value is related to the surface roughness and for an ideally flat electrode is equal to 1 and parameter $T = C_{dl}$ for $\phi = 1$.

* On leave from Department of Pharmacy, Medical University, 50-139 Wrocław, Poland

0021-891X © 1993 Chapman & Hall

In this study as well as in the previous one [13], the CPE model gives the best approximation of the experimental a.c. curves. In this model, the double layer capacity is replaced by the CPE. The approximation was carried out using a modified version of the complex nonlinear least square fitting program (CNLS) written by Macdonald *et al.* [22]. The values of parameters A, T and ϕ were determined from a.c. measurements. Parameter A is equal to $1/R_{ct}$, where R_{ct} is the charge-transfer resistance. The nonlinear least square fitting (NLS) procedure of the dependences of $\log i$ (from steady-state polarization measurements) and $\log A$ on the overpotential was used to determine the HER mechanism and the kinetic parameter values. The details of our approximation procedure were shown in many references [23–26].

3. Experimental details

3.1. *Preparation of the binder*

Lanthanum phosphate was produced by combining acid lanthanum phosphate and lanthanum hydroxide [12]. Two overall reactions are involved in the formation of acid phosphate lanthanum $La(H_2PO_4)_3$ and its subsequent transformation into $LaPO_4$:

$$\tfrac{1}{2}La_2O_3 + 3H_3PO_4 \longrightarrow La(H_2PO_4)_3 + \tfrac{3}{2}H_2O \quad (5)$$

$$La(H_2PO_4)_3 + 2La(OH)_3 \longrightarrow 3LaPO_4 + 6H_2O \quad (6)$$

The $La(H_2PO_4)_3$ was synthesized by adding 48.88 g La_2O_3 to 103.7 g H_3PO_4 (85%) in a rectangular Teflon cell measuring 10 cm × 5 cm × 5 cm, since a reactive intermediate reacts with glass rather than Teflon. The reactive mixture was stirred constantly during the addition of La_2O_3 until a very thick, silicon-like paste was obtained. Because the reaction is very fast, strongly exothermic and autocatalytic, even when the components are mixed at room temperature, the La_2O_3 must be completely incorporated within a few minutes. As soon as the reaction ended, the Teflon reactor was heated in an oven at 150° C for 24 h. The reaction product, in the form of a viscous paste, was transferred to a flask and vacuum-dried to remove traces of water resulting from the reaction. The addition of 0.883 g $La(OH)_3$ per 1 g of $La(H_2PO_4)_3$ made it easier to crush and mix the two components in a ball mill. The mixture was stored for several days in a dessicator before final polymerization. It should be noted that polymerization is very slow at room temperature.

3.2. *Deposition of ruthenium on nickel particles*

The spiky filamentary nickel particles (Inco 225) were put into a beaker containing 50 ml of Barnstead Nanopure water. The solution was deaerated by bubbling nitrogen. Nickel particles were added to the solution containing the appropriate amount of $RuCl_3 \cdot 6\,H_2O$ (Aldrich Co.). A few drops of concentrated HCl were added to the solution to solubilize ruthenium complexes when necessary. The red–ox reactions to obtain ruthenium deposited onto nickel particles are [15]:

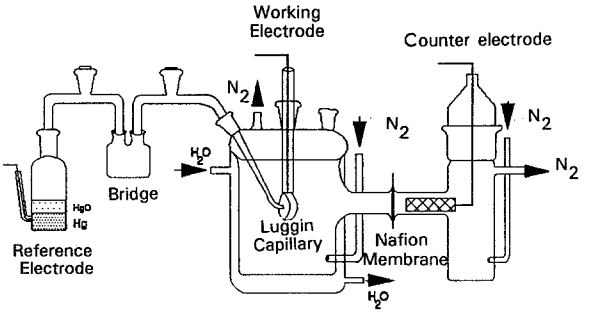

Fig. 1. Schematic representation of the electrochemical cell.

$$RuCl_6^{3-}(aq) + 3e^- \longrightarrow Ru + 6\,Cl^-(aq) \quad (7)$$

$$Ni \longrightarrow Ni^{2+} + 2e^- \quad (8)$$

and the overall reaction is:

$$3\,Ni + 2\,RuCl_6^{3-} \longrightarrow 2\,Ru + 3\,Ni^{2+} + 12\,Cl^- \quad (9)$$

The colour of the solution changed during the deposition from black to blue because of the formation of ruthenium (II) intermediate [15] and then became green due to the presence of dissolved nickel; it was an indication of the end of the reaction. U.v./vis. analysis of the solution showed the complete disappearance of ruthenium complexes from the solution and X-ray fluorescence of the electrode materials confirmed that all the ruthenium initially present in the solution is deposited.

3.3. *Preparation of the electrodes*

The mixture of the $La(H_2PO_4)_3$ and $La(OH)_3$ with Ni/Ru powder was pressed under vacuum in a mould 1.3 cm in diameter to obtain pellets [10–13]. A nickel foil was introduced to ensure a proper electrical contact. Polymerization was achieved by heating the pellets for 3–4 h under a flow of argon at different temperatures (200–800° C) after 12 h of preheating at 120° C. The electrodes were coated on one side and on the edge with Epofix resin (Struers). The obtained disc geometric surface area was 1.33 cm^2. The contents of ruthenium in the electrode materials were 1, 2, 3.5, 5, or 10 wt % as compared to 2 wt % for the binder ($LaPO_4$), and the rest of 100 wt % was nickel. The polymerization process was described in detail in previous papers [10, 12, 13].

3.4. *Electrochemical studies*

The experiments were performed in a dual-compartment glass cell (Fig. 1) separated by a Dupont Nafion® membrane 901 (Electrosynthesis Co.). The temperature of the cell compartment containing the working electrode was kept constant by circulating thermostated water. A Luggin capillary tube was placed less than 1 mm from the vertically placed working electrode. A nickel grid with a projected geometric

surface area of 40 cm^2 was used as a counter electrode, and the reference was a Hg/HgO/1 M KOH electrode. The measured value of the reversible potential of the HER in 1 M KOH was −925 mV compared to the reference electrode at 25° C. Barnstead Nanopure water with 17.5 MΩ cm resistivity was used to prepare KOH (Fischer-certified ACS reagent grade) and NaOH (Aldrich semiconductor grade 99.99%) solutions, which were deaerated by nitrogen bubbling.

The steady state and a.c. measurements were made by galvanostat-potentiostat PAR 273 and EG&G 5208 lock-in analyser controlled by a Commodore PC2.

3.5. *Determination of kinetic parameters*

Cathodic polarization curves were obtained by decreasing the applied current galvanostatically from 250 to 0.01 mA cm^{-2} after ~2 h under a cathodic current of 250 mA cm^{-2}. The electrode potentials were corrected for the ohmic drop by the current-interruption and the a.c. impedance techniques. Both methods gave similar results [12, 24]. No differences were observed in cathodic polarization curves registered after 2 h polarization under 250 mA cm^{-2} in both 1 M KOH and NaOH solutions.

In another set of experiments, the a.c. measurements were carried out after approximately 30 cycles, each cycle consisting of 30 min of galvanostatic electrolysis at 125 mA cm^{-2} and 10 min of Tafel curve measurement at cathodic current densities from 250 mA cm^{-2} to 10^{-5} mA cm^{-2}. After such treatment, all Tafel parameters became constant with further cycles and reproducible a.c. measurements were obtained, i.e. the variation on the Tafel slope was within ~2%, compared to ~10% for the exchange current density. In this experiment 1 M NaOH (Aldrich semiconductor grade 99.99%) solutions were used to avoid the long term influence of the impurities on the kinetic parameters evaluation of the HER.

The Tafel parameters for the OER were obtained for Ni/Ru electrodes at 25° C after 30 min under an anodic current density of 250 mA cm^{-2} at 70° C. This procedure was chosen to obtain reproducible steady-state polarization measurements at 25° C. The reversible potential for the OER was +304 mV vs Hg/HgO. On the basis of XRF studies it was noticed that a large part of ruthenium is dissolved in the electrolyte after preanodization at 70° C. It is consistent with the large solubility of the ruthenium oxide or complexes, [15, 27, 28].

4. Results and discussion

4.1. *Materials characterization*

The polymerization of $LaPO_4$ may be performed at various temperatures. It was found that the change in the polymerization temperatures from 300 to 800° C may induce changes in the Ru/Ni powder. Differential Thermal Analysis (DTA) of the ruthenium deposited on nickel powder showed that the phase changes occur at 275 and 700° C (Fig. 2). Examples of XRD diffractograms of Ru(10 wt %)/Ni powders, which were dried at 100° C during 12 h after ruthenium deposition and then heated at 400 and 700° C in argon atmosphere, are presented in Fig. 3. The X-ray fluorescence analysis showed that the powder obtained after the deposition process contained ~10 wt % of ruthenium while the XRD ruthenium lines were not observed before heat treatment. After the heating of powder at 400° C in an inert atmosphere, ill-defined peaks of NiO and Ru appeared (Fig. 3). The broadening of the peaks was connected with the emergence of small particles of NiO and Ru. In addition, there was a wide band of weak intensity in the region of $2\theta = 27°$ on the XRD spectra, which is characteristic of an amorphous structure. Spectrum in Fig. 3 obtained for Ru/Ni powder heated at 700° C proved that NiO and Ru possessed a well-defined crystalline structure. Similar changes from a disordered to ordered structure during heating are well-known [29].

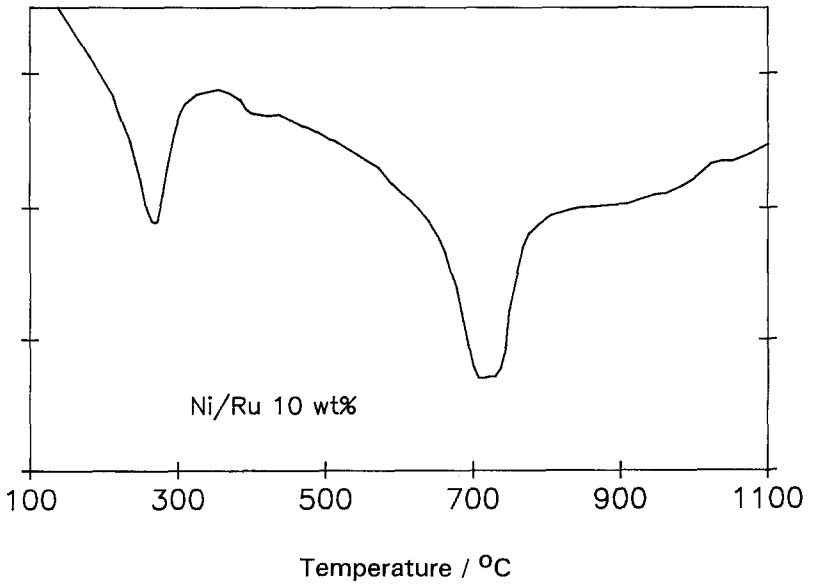

Fig. 2. Differential thermal analysis of ruthenium deposited on nickel powder.

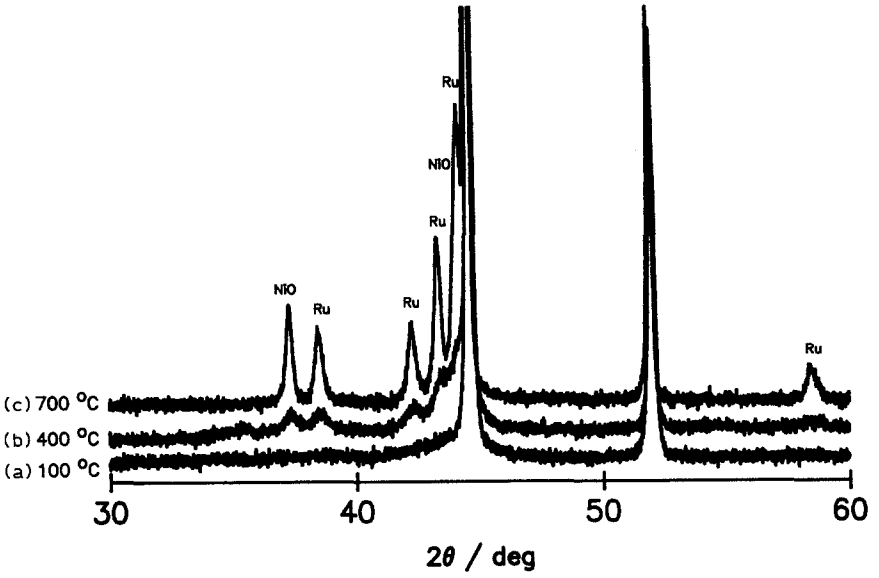

Fig. 3. X-ray powder diffraction spectrum: (a) for Ni/Ru powder heated at 100° C; (b) for Ni/Ru powder heated at 400° C; and (c) for Ni/Ru powder heated at 700° C.

The above results of X-ray powder diffraction (Fig. 3) suggested that the first DTA transition is associated with the reaction of an amorphous form of Ru_xO_y obtained by reducing the ruthenium complex on the nickel surface with nickel according to the reduction reaction:

$$Ru_xO_y + yNi = yNiO + xRu \qquad (10)$$

As predicted from thermodynamic data, the free energy of the reduction reaction of the most stable ruthenium oxide is approximately equal to $-250\,kJ\,mol^{-1}$ in a temperature range of 100 to 600° C [30]. The reaction does not occur at the lower temperature (no XRD lines of NiO and Ru) because of kinetic limitations. On the other hand it was shown in [31] that the production of ruthenium metal by thermal decomposition of RuO_2 did not occur even after vacuum heating at 725° C for 2 h.

The energy dispersive X-ray (EDX) mapping (electron microbe in SEM) made on a cross section of Ni/(10 wt %) Ru particles previously heated at 300° C (typical polymerization temperature) suggested the formation of ruthenium oxide covering the nickel particles (Fig. 4). The XRF studies indicate that the total amount of ruthenium dissolved in solution was deposited on the surface of the nickel particles. The EDX mapping of the cross section showed that ruthenium is present on the particle surface only. The mapping also showed larger amounts of oxygen in the ruthenium layer. These findings, along with the DTA results, indicate that Reaction 10 is taking place. Besides, XRD measurements showed that Ru and NiO peaks appear only after heating the powder at 400 and

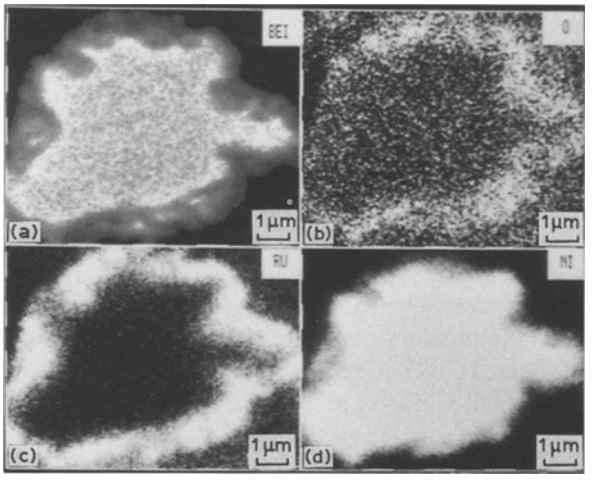

Fig. 4. Energy dispersive X-ray mapping pictures of Ni/Ru particles cross-section. (a) Backscattered electron picture. (b) Oxygen X-ray mapping of sample from picture 3a. (c) Ruthenium X-ray mapping of the same sample. (d) Nickel X-ray mapping of the same sample.

Table 1. Specific surfaces and roughness factor of materials obtained from BET measurement

Powder types	*Heating* temperature* °C	*Specific† surface* $m^2\,g^{-1}$	*Roughness factor*
Ni[1]	RT‡	0.6	–
Ni[2]	250	–	4400§
Ni[1]	300	0.6	–
Ni[1]	400	0.55	3900§
Ni/Ru 1.0%	RT	2.5	10000**
Ni/Ru 2.0%	RT	2.7	8200**
Ni/Ru 5.0%	RT	4.5	10600**
Ni/Ru 10%	RT	7.3	58000**
Ni/Ru 1.0%	300	–	8000§
Ni/Ru 3.5%	300	–	7100§
Ni/Ru 5.0%	300	4.3	
Ni/Ru 5.0%	400	1.6	
Ni/Ru 5.0%	600	1.0	

* for ~3 h under argon atmosphere
† metal powders
‡ RT: room temperature, no heat treatment
§ polymerized LPBN electrodes
** unpolymerized $La(H_2PO_4)_3$ and $La(OH)_3$ pressed with metal powder
[1] From [13]
[2] From [11]

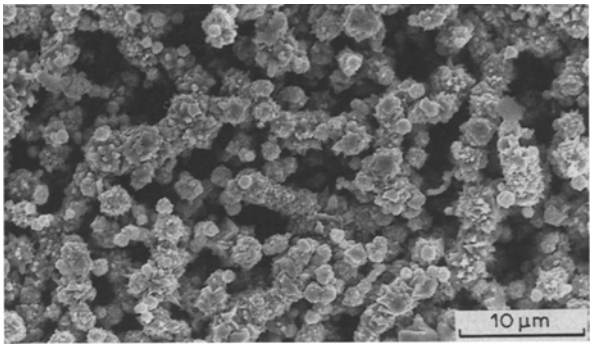

Fig. 5. SEM picture of LPBN–Ru 3.5 wt % polymerized at 300° C.

700° C under an argon atmosphere. The peaks for NiO were absent when nickel powder or rhodium on nickel [13] was heated under the same experimental conditions. The results indicate that the deposition of ruthenium lead initially to the formation of an oxide Ru_xO_y on a nickel surface which at higher temperature may be reduced to a metallic ruthenium.

The real surface area of Ru/Ni powders and the associated roughness factor of the electrodes containing from 0 wt % to 10 wt % of ruthenium measured by BET technique are illustrated in Table 1. Surface roughness factor values for dried metal powders with $La(H_2PO_4)_3$ and $La(OH)_3$ (room temperature) and the electrodes polymerized at various temperatures are also presented. These results are in good agreement with previous studies on such materials [13], showing that the surface area decreases with an increase in the polymerization temperature and increases with an increase in ruthenium content. It should be noticed that the specific surface of LPBN and LPBN–Ru(5 wt %) electrodes is unaffected by heating up to 400° C, which suggests that the specific area of the pellets before (Table 1) and after polymerization at 300° C are approximately the same. A SEM picture of a Ni/Ru 3.5% polymerized at 300° C before electrolysis is presented in Fig. 5. The fractal shape of the powder and the porous nature of the electrode surface are noticed.

Table 2. Effect of temperature and ruthenium content on HER kinetic parameters of nickel powder electrodes at 25° C in 1 M KOH and NaOH

Ru/%	*300° C*			*400° C*			*600° C*		
	b	I_o	η_{250}	*b*	I_o	η_{250}	*b*	I_o	η_{250}
0.0[1]	132	12	177	130	3.1	257	114	0.3	334
1.0	64	54	42	108	20	120	122	13.8	155
2.0	–	–	–	99	15	122	–	– /	–
5.0	40	25	39	106	24	108	104	9.5	148
10.0				32	47	23			
Ru[2]				68	50	55			

b Tafel slope (mV dec^{-1})
I_o Exchange current density (mA cm^{-2})
η_{250} Overpotential at 250 mA cm^{-2} (mV)
[1] LPBN electrodes from [13]
[2] $LaPO_4$ bonded Ru electrode

Table 3. HER Tafel parameters after multicycle polarization experiment at 25° C in 1 M NaOH

Composition /wt %	*Temp.* /° C	*Tafel slope* /mV dec^{-1}	*Exchange current density* /mA cm^{-2}	*Overpotential at 250 mA cm^{-2}* /mV
Ni[1]	300	124	4.2	216
Ni[1]	600	118	0.3	283
Ni–Ru(3.5)	300	70	34	60
Ni–Ru(3.5)	600	140	8	205

[1] LPBN electrode from [13].

4.2. *Kinetics of the HER*

Tafel curves were obtained for the HER on Ni/Ru powder electrodes for different polymerization temperatures. The kinetic parameters and the electrocatalytic activity at 250 mA cm^{-2} are summarized in Table 2. These electrodes show considerable improvement in the electrocatalytic activity at 250 mA cm^{-2} compared to the nickel powder lanthanum phosphate bonded electrodes described in previous works [10, 11].

The most active electrodes were obtained at the lower polymerization temperature, i.e. 300° C. Electrodes containing 1 wt % Ru and polymerized at 300° C have Tafel parameters similar to those made of pure ruthenium powder and containing the same amount of $LaPO_4$. In the latter case, the following Tafel parameters were obtained: $i_o = 50$ mA cm^{-2}, $b = 68$ mV dec^{-1} and $\eta_{250} = -55$ mV. As shown in Table 3, a slight decrease in electrocatalytic activity was observed during the multicycle experiment for Ni/(3.5 wt %)Ru electrodes.

Ruthenium–nickel electrodes containing 3.5 wt % Ru were chosen for a detailed electrochemical investigation in order to compare their characteristics to those obtained with Ni/Rh electrodes [13]. One semicircle on the complex plane impedance plot was found for the electrode polymerized at 600° C and two semicircles for Ni–Ru powder electrodes prepared at 300° C. The second semicircle was so perturbed that it was impossible to determine its parameters and the analysis was carried out using only the first semicircle. Sample Nyquist graphs obtained on LPBN–Ru(3.5 wt %) electrodes polymerized at 600° C are shown in Fig. 6. The real and imaginary components Z' and Z'' obtained for all frequencies at various d.c. potentials were analysed using the complex nonlinear least squares fitting program (CNLS) written by Macdonald *et al.* [22] and modified in order to find the experimental values of parameters A, T, ϕ and R_s. Figure 4 shows that the experimental complex-plane impedance diagrams are very well fitted by the CNLS approximation. The results of approximation of $\log i$ (from Tafel curves) and $\log A$ against overpotential dependences are presented in Figs 7 and 8. It was found that the HER proceeds via Volmer–Heyrovsky reaction with the value of $k_1 \ll k_2$; it was impossible to determine the exact value k_2, because the standard deviation was higher than the rate constant value. In

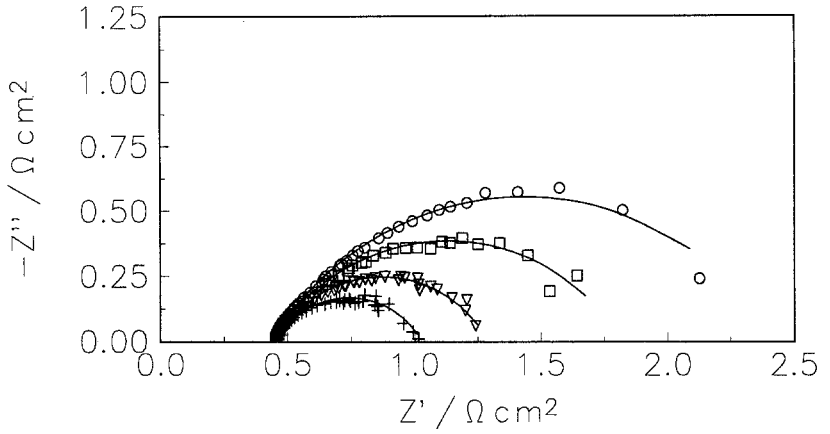

Fig. 6. Experimental (points) and simulated (solid lines) values of Z'' against Z' in 1 M NaOH at 25° C for LPBN–Ru (3.5 wt %) electrode polymerized at 600° C. Key: (○) −80 mV, (□) −110 mV, (▽) −130 mV, and (+) −160 mV.

addition, the Volmer–Heyrovsky reaction mechanism has two solutions [24]: exchanging the rate constants k_1 and k_2, k_{-1} and k_{-2} and α_1 and α_2, leaves all the experimental curves for all the techniques unchanged, and the only difference is in the calculated surface coverage by adsorbed hydrogen. The kinetic parameters of the HER are presented in Table 4.

The capacity of the double layer presented in Fig. 9 was calculated according to the following equation [21]:

$$T = C_{dl}^{\phi}(R_s^{-1} + A)^{(1-\phi)} \qquad (11)$$

The roughness factor R was estimated from the experimental values of capacity of the double layer divided by the capacity of the smooth metal surface, which equals 20 μF cm^{-2} (Table 5) [23]. The roughness factor for Ni/Ru electrodes prepared at 300° C is approximately 1.5 times higher than for similar Ni/Rh electrodes [13], and identical for Ni and Ni/Ru 3.5 wt % electrodes heated at 600° C. On the other hand the values of rate constants obtained for Ni and Ni/Ru electrodes at lower (300° C) temperature are a few orders of magnitude higher than for the same electrodes prepared at 600° C. The addition of ruthenium to pure nickel electrodes considerably improves its electrocatalytic activity only if the polymerization temperature is low, i.e. 300° C. The electrochemically determined roughness factor is much smaller than that determined by BET method. The electrochemical roughness factor is related to the electrode–solution interface. By contrast, the surface area obtained by BET measurements is larger compared to the former one since it is related to the surface accessible for gas adsorption. Also, however the electrochemically active surface area may drop at high rate of gas evolution as the current density increase (Fig. 9).

A strong influence of polymerization temperature is evidenced considering the intrinsic electrocatalytic activity, i.e. when the rate constants divided by the roughness factor are taken into account. The rate constants per real surface area k_1/R, determined on the LPBN electrode decrease as the temperature increases from 300° to 600° C (Table 5). The same observation is valid for LPBN/Ru electrodes. When the electrocatalytic behavior of Ni and Ni/Ru electrodes are compared, the effect of ruthenium on the

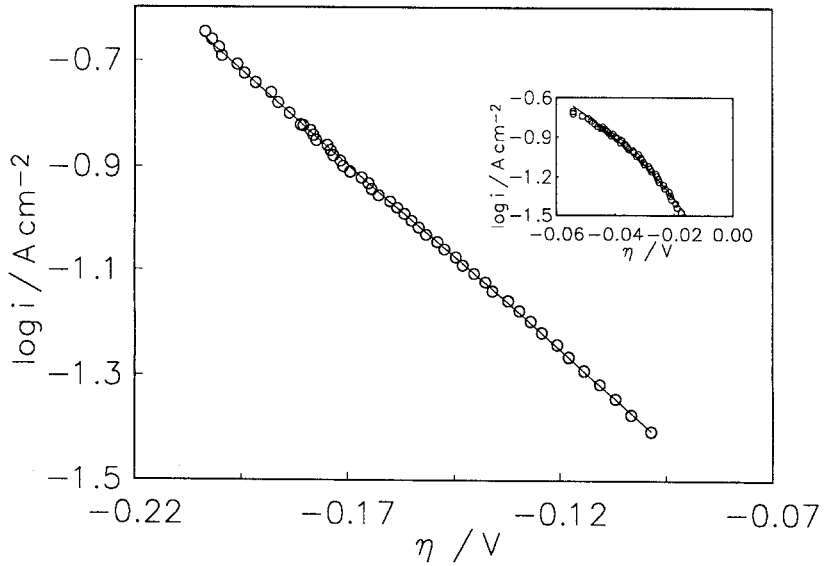

Fig. 7. Tafel plots obtained in 1 M NaOH at 25° C on nickel–ruthenium (3.5 wt %) electrode polymerized at 600° C and insert at 300° C, (—) calculated.

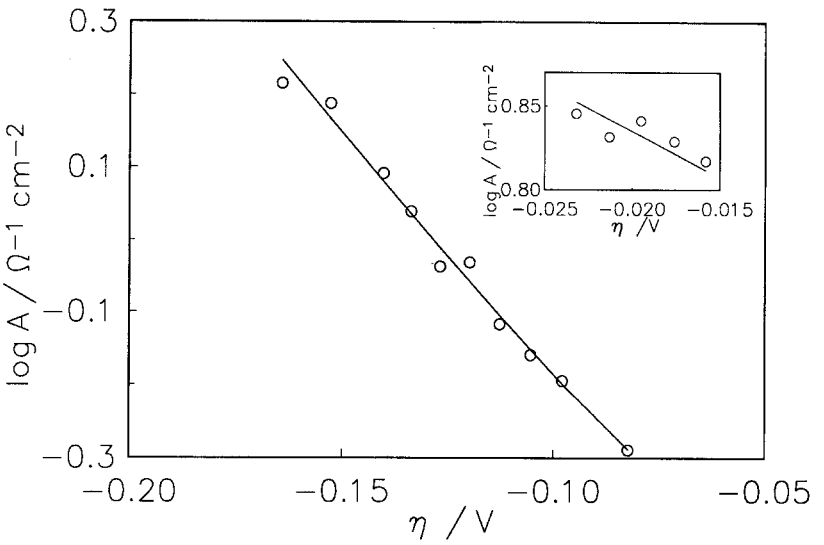

Fig. 8. Dependence of the logarithm of parameter A on the overpotential in 1 M NaOH at 25° C: nickel–ruthenium (3.5 wt %) electrode polymerized at 600° C and insert at 300° C, (—) calculated.

electrocatalytic properties is evident. The highest activity corresponds to the Ni/Ru electrodes polymerized at 300° C. The presence of ruthenium increases the k_1/R ratio by a factor of ten as compared to the LPBN electrode (Ni without Ru). It was reported earlier [13] that an increase of temperature to 600° C causes melting of the needles on Ni or Ni/Rh particles resulting in a decrease of electrocatalytic activity. Based on these results, it was deduced that improvement of performances of nickel powder electrodes when nickel particles are encapsulated with ruthenium is related to an increase of both the roughness factor and the intrinsic electrocatalytic activity of the electrode material. It should be pointed out that the same conclusion was drawn for Ni/Rh electrodes. The values of the rate constants divided by the roughness factor (Table 5) are approximately the same for Ni/Ru and Ni/Rh electrodes prepared at 300° C. The difference is that ruthenium does not create a solid homogenous solution with nickel at temperatures below 800° C and the Ni/Ru electrode heated at 600° C is substantially more active than similar Ni/Rh and Ni electrodes prepared under the same experimental conditions [13]. It could be concluded that the high activity of Ni/Rh and Ni/Ru electrodes is related to the presence of particles of a more active metal or its oxide. The alloying process can significantly decrease the activity of the mixed electrodes. A similar difference was found in the case of polymer-bonded composite nickel electrodes [4].

4.3. *Kinetics of the OER*

Since ruthenium oxide is well-known as anode material in water electrolysis [32, 33], it led us to evaluate the performance of the OER of LPBN–Ru electrodes. OER kinetic parameters for the Ni/Ru electrode were slightly affected by the polymerization temperature up to 600° C (Table 6). The Tafel slope and the exchange current density for the OER were significantly affected by ruthenium content up to 5 wt % compared to nickel powder electrodes [12, 13]. The drop of the Tafel slope with the augmentation of ruthenium content results in a decreased oxygen overpotential at 250 mA cm^{-2}. Since ruthenium dissolves in a basic medium to form RuO_4^{2-} [15, 27, 28], it may induce an increase of the specific surface area which results in an improvement of electrocatalytic activity. On the other hand it is anticipated that the intrinsic electrocatalytic activity for the OER will decrease with time due to the removal of ruthenium. The use of lanthanum phosphate-bonded composite nickel–ruthenium anodes in base are not attractive owing to the tendency of ruthenium to corrode; long term experiments for OER on LPBN–Ru electrodes were thus not considered.

Table 4. Rate constant values obtained from a.c. measurements at 25° C in 1 M NaOH

Composition /wt %	*Temp.* /° C	$k_1 \times 10^8$ /mol cm^{-2} s^{-1}	$k_{-1} \times 10^8$ /mol cm^{-2} s^{-1}	$k_2 \times 10^7$ /mol cm^{-2} s^{-1}	α_1	α_2
Ni[1]	300	2.86 ± 0.61	2.92 ± 2.63	1.04 ± 0.73	0.46 ± 0.01	†
Ni[1]	600	0.21 ± 0.01	*	*	0.51 ± 0.01	†
Ni–Ru(3.5)	300	117 ± 10	*	*	0.49 ± 0.11	†
Ni–Ru(3.5)	600	4.13 ± 1.01	*	*	0.42 ± 0.02	0.36 ± 0.02

* Very large values, precise determination is questionable
† $\alpha = 0.5$ was assumed
[1] LPBN electrodes from [13]

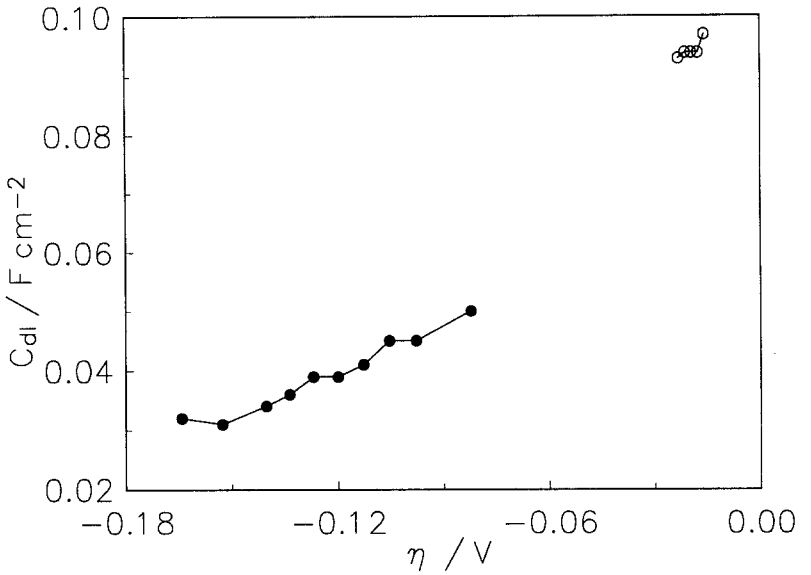

Fig. 9. Dependence of the double-layer capacity on the overpotential: nickel–ruthenium (3.5 wt %) electrode polymerized at 600° C (●) and at 300° C (○).

Table 5. Rate constant values divided by surface roughness factor at 25° C in 1 M NaOH

Composition /wt %	*Polymerization temperature* /° C	*Roughness factor**	$(k_1/R) \times 10^{10}$ /mol cm^{-2} s^{-1}
Ni pure[1]	300	1000	0.286
Ni pure[1]	600	1650	0.013
Ni-Ru(3.5)	300	4700	2.520
Ni-Ru(3.5)	600	1600	0.258

* From double layer capacity measurements
[1] From [13]

5. Conclusions

It was shown that the lanthanum phosphate-bonded nickel/ruthenium electrodes are very active for the HER over ruthenium contents ranging from 0 to 10 wt %. The steady state HER overpotential at 250 mA cm^{-2} in 1 M alkaline solution was approximately 45 mV for 1 wt % of Ru electrode polymerized at 300° C. Tafel parameters and η_{250} for LPBN electrodes with Ni/Ru powders are practically similar to those prepared with pure ruthenium, the content in the $LaPO_4$ being the same. It was shown that the ruthenium deposited on nickel particles forms an amorphous oxide. A heat treatment of the powder is favourable for reducing ruthenium oxide by nickel substrate. The improvement of nickel powder electrode electrocatalytic activity is related to the presence of a more active metal or its oxide covering nickel powder particles. The HER proceeds via the Volmer–Heyrovsky reaction with one rate-determining step. The constant phase element model was applicable for the a.c. impedance measurement fitting.

Acknowledgements

We would like to acknowledge the Natural Science and Engineering Research Council of Canada, IREQ and the Quebec government for their financial support. Special thanks to Mr L. Timberg of Inco Metals Company for furnishing the characterized nickel powders and J. Naud and P. Magny for their help at various stages of this work.

References

[1] D. E. Hall, *J. Electrochem. Soc.* **128** (1981) 740.
[2] B. E. Conway, H. Angerstein-Kozlowska and M. A. Sattar, *ibid.* **130** (1983) 1825.
[3] D. E. Brown, N. M. Mahmood, M. C. Man and A. K. Turner, *Electrochim. Acta* **29** (1984) 1551.

Table 6. Effect of temperature and ruthenium content on OER parameters of nickel powder electrodes at 25° C in 1 M KOH and NaOH

Ru/%	300° C			400° C			600° C		
	b	$I_o \times 10^{-3}$	η_{250}	b	$I_o \times 10^{-3}$	η_{250}	b	$I_o \times 10^{-3}$	η_{250}
0.0[1]	109	14	463	96	7	438	–	–	–
1.0	96	65	343	94	67	378	93	12	404
2.0	–	–	–	101	76	356	–	–	–
5.0	79	80	272	83	63	299	83	70	295
10.0				64	47	238			

b Tafel slope (mV dec^{-1})
I_o Exchange current density (mA cm^{-2})
η_{250} Overpotential at 250 mA cm^{-2} (mV)
[1] LPBN electrodes from [13]

[4] D. E. Hall, *J. Appl. Electrochem.* **14** (1984) 107.
[5] M. Bica de Moares, D. M. Soares and O. Teschke, *J. Electrochem. Soc.* **131** (1984) 1931.
[6] B. E. Conway and L. Bai, *Int. J. Hydrogen Energy* **11** (1986) 533.
[7] E. Endoh, H. Otouma, T. Morimoto and Y. Oda, *ibid.* **12** (1987) 473.
[8] S. Trasatti, *in* 'Advances in Electrochemical Science and Engineering', (edited by H. Gerisher and C. W. Tobias), Vol. 2, VCH, Weinheim (1992) p.1.
[9] H. Wendt (Ed.), 'Electrochemical Hydrogen Technologies', Elsevier Scientific, Amsterdam (1990) p.29.
[10] E. Potvin, H. Ménard, J. M. Lalancette and L. Brossard, *J. Appl. Electrochem.* **20** (1990) 252.
[11] E. Potvin, A. Lasia, H. Ménard and L. Brossard, *J. Electrochem. Soc.* **138** (1991) 900.
[12] H. Dumont, P. K. Wrona, L. Brossard, J. M. Lalancette and H. Ménard, *J. Appl. Electrochem.*, in press.
[13] H. Dumont, P. Los, L. Brossard, A. Lasia and H. Ménard, *J. Electrochem. Soc.* **139** (1992) 2143.
[14] B. V. Tilak, A. C. Ramamurthy and B. E. Conway, *Proceedings of the Indian Academy of Science (Chemical Science)*, **97** (1986) 359.
[15] J. F. Lopis and M. Tordesillas, *in* 'Encyclopedia of Electrochemistry of the Elements', (edited by A. J. Bard), Vol. 6, M. Dekker, New York (1975) p.277.
[16] T. Pajkossy, *J. Electroanal Chem.* **300** (1991) 1.
[17] V. Rammelt and G. Reinhard, *Electrochim. Acta* **35** (1990) 1045.
[18] M. Keddam and H. Takenouti, *ibid.* **33** (1988) 445.
[19] T. Pajkossy and L. Nyikos, *J. Electrochem. Soc.* **133** (1986) 2061.
[20] R. de Levie, *J. Electroanal. Chem.* **261** (1984) 1.
[21] G. J. Brug, A. L. G. van der Eeden, M. Sluyters-Rehbach and J. H. Sluyters, *ibid.* **176** (1984) 275.
[22] J. R. Macdonald, J. Schoonman and A. P. Lehner, *ibid.* **131** (1982) 77.
[23] L. Chen and A. Lasia, *J. Electrochem. Soc.* **138** (1991) 332.
[24] A. Lasia and A. Rami. *J. Electroanal. Chem.* **294** (1990) 123.
[25] Y. Choquette, L. Brossard, A. Lasia and H. Ménard, *J. Electrochem. Soc.* **137** (1990) 1723.
[26] Y. Choquette, L. Brossard, A. Lasia and H. Ménard, *Electrochim. Acta* **35** (1990) 1251.
[27] N. de Zoubov and M. Pourbaix, 'Rapports Techniques', No. 58, Cebelcor, Brussel, (1958).
[28] J. Llopis, *Anal. Real Soc. Espan. Fis. Quim., Ser. B* **61** (1965) 355.
[29] S. Mukerjee, *J. Appl. Electrochem.* **20** (1990) 537.
[30] CRC Handbook of Chemistry and Physics, (edited by R. C. Weast), 67th edn., Florida (1986–87).
[31] M. S. Hegde, T. S. Sampath Kumar and R. M. Mallya, *Surf. Sci.* **188** (1987) 255.
[32] F. Gutmann and O. J. Murphy, *in* 'Modern Aspects of Electrochemistry', No. 15, (edited by R. E. White, J. O'M. Bockris and B. E. Conway), Plenum Press, New York (1983).
[33] L. I. Yurkov, V. B. Brusse-Macukas, F. I. Lvovich, V. L. Kubasov, A. F. Mazanko and N. S. Fedotova, *U.S. Patent, 4 589 969* (1986).